NIH Public Access
Author Manuscript
Eur J Neurosci. Author manuscript; available in PMC 2011 October 1.

Published in final edited form as:
Eur J Neurosci. 2010 October ; 32(7): 1223–1238. doi:10.1111/j.1460-9568.2010.07376.x.

β-Secretase-1 elevation in aged monkey and Alzheimer's disease human cerebral cortex occurs around vasculature in partnership with multisystem axon terminal pathogenesis and β-amyloid accumulation

Yan Cai[1,2,#], **Kun Xiong**[1,#], **Xue-Mei Zhang**[3,4,#], **Huaibin Cai**[5], **Xue-Gang Luo**[1], **Jia-Chun Feng**[4], **Richard W. Clough**[3], **Robert G. Struble**[6], **Peter R. Patrylo**[2,3], **Yaping Chu**[7], **Jeffrey H. Kordower**[7], and **Xiao-Xin Yan**[3,*]

[1]Department of Anatomy and Neurobiology, Central South University Xiangya Medical School, Changsha, Hunan, China

[2]Department of Physiology, Southern Illinois University School of Medicine, Carbondale, IL, USA

[3]Departments of Anatomy, Southern Illinois University School of Medicine, Carbondale, IL, USA

[4]Department of Neurology, The First Hospital of Jilin University, Changchun, Jilin, China

[5]Laboratory of Neurogenetics, National Institute on Aging, National Institutes of Health, Bethesda, MD, USA

[6]Center for Alzheimer's disease, Southern Illinois University School of Medicine, Springfield, IL, USA

[7]Department of Neurological Sciences, Rush University Medical Center, Chicago, IL, USA

Abstract

Alzheimer's disease (AD) is the most common dementia-causing disorder in the elderly, which may relate to multiple risk factors and is pathologically featured by cerebral hypometabolism, paravascular β-amyloid (Aβ) plaques, neuritic dystrophy and intra-neuronal aggregation of phosphorylated-tau. To explore potential pathogenic link among some of these lesions, we examined β-secretase-1 (BACE1) alteration relative to Aβ deposition, neuritic pathology and vascular organization in aged monkey and AD human cerebral cortex. Western blot analyses detected increased levels of BACE1 proteins and β-site-cleavage amyloid precursor protein C-terminal fragments in plaque-bearing human and monkey cortex relative to controls. In immunohistochemistry, locally elevated BACE1 immunoreactivity (IR) occurred in AD but not in control human cortex, with a trend of increased overall density among cases with greater plaque pathology. In double labeling preparations, BACE1 IR colocalized with immunolabeling for Aβ but not for phosphorylated tau. In perfusion-fixed monkey cortex, locally increased BACE1 IR co-existed with intra-axonal and extracellular Aβ IR among virtually all neuritic plaques ranging from primitive to typical cored forms. This BACE1 labeling localized to swollen/sprouting axon terminals that might co-express one or another neuronal phenotype marker (GABAergic, glutamatergic, cholinergic or catecholaminergic). Importantly, these BACE1-labeled dystrophic axons resided near or in direct contact with blood vessels. These finds implicate that plaque formation in AD or normal aging primates relate to a multisystem axonal pathogenesis that occurs

[*]Correspondence to: Xiao-Xin Yan, Department of Anatomy, Southern Illinois University School of Medicine at Carbondale, 1135 Lincoln Drive, 2069 Life Science III, Carbondale, IL 62901-6525. Tel: 618-453-1527; xyan@siumed.edu.
[#]Authors contributed equally to this study

NIH-PA Author Manuscript
NIH-PA Author Manuscript
NIH-PA Author Manuscript

NIH-PA Author Manuscript

NIH-PA Author Manuscript

NIH-PA Author Manuscript

in partnership with potential vascular or metabolic deficit. The data provide a tangible mechanistic explanation as to why senile plaques are present preferentially near cerebral vasculature.

Keywords

Neuritic plaque; neuroplasticity; hypometabolism; aging; dementia; non-human primate

Introduction

β-Amyloid peptide (Aβ) deposition in extracellular space, referred to as amyloid or senile plaques, represents a principal neuropathology of Alzheimer's disease (AD). Amyloid plaques in cerebral parenchyma may exhibit complex morphological configuration in histological (e.g., Bielschowsky, Congo red and thioflavin stains) or immunohistochemical preparation (Dickson and Vickers, 2001; Thal et al., 2006; Duyckaerts et al., 2009). Plaques appear to contain a mixer of Aβ products, including Aβ40 and Aβ42, their (C- and N-terminal) truncated and elongated (Aβ43 to Aβ48) versions, and oligomerized and fibrized forms of these peptides (Welander et al., 2009; Sarsoza et al., 2009; Härtig et al., 2010; Portelius et al., 2010; van Helmond et al., 2010). Parenchymal plaques may be generally divided into diffuse and neuritic forms, with the latter typically associated with dystrophic neurites (Fiala, 2007; Duyckaerts et al., 2009). A prominent anatomic feature of neuritic plaques is their preferential distribution near blood vessels (Miyakawa et al., 1982; Kawai et al., 1990, 1992). Amyloid deposition can also occur in the wall of blood vessels (Weller et al., 2009), which might develop during Aβ clearance from the brain into the blood stream, since Aβ immunization appears to exacerbate cerebral amyloid angiopathy while facilitating the removal of parenchymal plaques (Boche et al., 2008).

Overall, plaque formation is thought to occur because of Aβ misfolding and/or an imbalance between its genesis and clearance (Neugroschl and Sano, 2010). It is interesting that major Aβ clearance molecules are actually elevated in aging and AD brain (Miners et al., 2010). During the past few years, evidence accumulates in supporting a key role for increased Aβ genesis in AD-type amyloidosis. Aβ production involves sequential proteolytic cleavages of β-amyloid precursor protein (APP) by β-secretase-1 (BACE1) and γ-secretase complex (Thinakaran and Koo, 2008). BACE1 messenger expression, protein levels, enzymatic activity and β-site APP cleavage product (β-site APP cleavage C-terminals, β-CTF or C99) are increased in AD brain and CSF relative to control (Zhong et al., 2007; Ewers et al., 2008; Zetterberg et al., 2008; Vassar et al., 2009; Mulder et al., 2010). Also, increased BACE1 immunoreactivity (IR) is detected around plaques in AD brain (Zhao et al, 2007).

In some transgenic mouse models of AD, neuritic plaques appear to develop in partnership with axonal swelling/sprouting intrinsically associated with BACE1 elevation (Zhang et al., 2009; 2010). In the present study we sought to explore amyloid plaque formation in AD human cerebral cortex by determining: (i) the anatomical distribution of BACE1 IR relative to Aβ accumulation; (ii) the cellular localization of increased BACE1 IR, especially its relevance to neuritic pathology; (iii) the spatial relationship of increased BACE1 IR to vasculature. The use of postmortem human tissue involves inherent pitfalls, especially autofluorescence and loss of antigenicity. Rhesus monkeys develop cerebral amyloid plaques with age, as with humans (Price et al., 1991; Sani et al., 2003, Roth et al., 2004). Perfused monkey tissues were therefore used in the present study to assess pathological profiles that are difficult to appraise in postmortem human brains.

NIH-PA Author Manuscript

NIH-PA Author Manuscript

NIH-PA Author Manuscript

Materials and Methods

Postmortem human cerebral cortex

Frozen frontal cerebral slices at the temporal lobe levels (~1 to 3 cm thick) prepared from clinically-diagnosed AD patients or aged individuals with and without a history of dementia were available for the present study, from Analytical Biological Services Inc. (ABC) (Wilmington, DE, USA) and the Alzheimer center of Southern Illinois University. A total of 17 cases of clinically-diagnosed AD or with a history of dementia (>3 years) and 14 non-demented cases, with postmortem delay ranged from 3 to 40 hours, were used for initial neuropathological screen using Bielschowsky silver stain, and phosphorylated tau (*p*-tau), Aβ and BACE1 immunohistochemistry (Supporting Fig. 1A-C). BACE1 immunolabeling tended to diminish in cortical samples (with amyloid plaques) with a postmortem delay ≥8 hours. Also, among the cases with clear cortical amyloidosis, tauopathy was not always observed. For these reasons, cortical samples were sorted, and the cases selected for the present study met the following conditions (Supporting Fig. 1-Table-1): (1) AD cases (n=7) showed both amyloid and tau pathologies, whereas control cases (n=7) were free of either lesion; (2) postmortem delays were less than 7 hours; (3) relatively well-preserved histological integrity as assessed with Nissl stain (Supporting Fig. 1A-I).

Perfused monkey cerebral cortex

Rhesus monkey (*Macaca mulatta*) brain materials were available from previous and ongoing other studies (Chu and Kordower, 2007). Frontal cortical sections across the anterioposterior dimension of the cerebrum from 7 mid-age to aged [23-34 year (yr)-old] monkeys were used to determine BACE1 localization and its relevance to amyloid and neuritic pathology in non-human primates. A hemispheric temporo-occipital block from each aged animal was also available, which was used for western blot and double-labeling studies. The monkey brains were perfused with normal saline followed by fixation with 4% paraformaldehyde, and the cerebral hemispheres were cut frozen (40 μm thick) on a sliding microtome at frontal plane. The monkey cortical samples had been stored in either cryoprotectant (sections) at −20°C or 30% sucrose (cortical blocks) at 4°C for a few months to 4 years before they were used in the present study. Animal use was in accordance with the National Institute of Health Guide for the Care and Use of Laboratory Animals, and was approved by Institutional Animal Care and Use Committee of Rush University.

Histology and immunohistochemistry

Human cortical samples were blocked to contain the cortex and white matter with an approximate volume of 1.5 (depth, relative to pia) × 2 (width) × 1 (thickness) cm^3, thawed at 4 °C and immersion-fixed with 4% paraformaldehyde in 0.01M phosphate-buffered saline (pH 7.4, PBS) overnight, followed by cryoprotection in 30% sucrose. The human and monkey cortical blocks were cut perpendicular to the pial surface at 40 μm using a cryostat, and adjacent sections were collected serially in PBS in 12-well culture plates. For plaque-bearing human and monkey brains, twelve sets of 20 μm (collected free-floating in PBS) and 12 sets of 8 μm (thaw-mounted on microslides) sections were also prepared, which were used for double labeling studies. Fiducial markers including needle punch and “corner-cutting” were made at different locations of the cortical blocks from different cases, which were used to sort sections from individual brains after an identical staining (i.e., batch-processing of sections from multiple cases).

For comparative qualitative and quantitative analyses, consecutive sets of sections (40 μm thick) from a set of AD (3-4 cases/batch) and control (3-4 cases/batch) cases were immunostained for BACE1 and two different Aβ antibodies (E50, 12F4 or 6E10, densitometry was based on 6E10 IR) with the peroxidase-3,3′-diaminobenzidine (DAB)

NIH-PA Author Manuscript

NIH-PA Author Manuscript

NIH-PA Author Manuscript

method. Antigen retrieval was processed for BACE1 labeling with 50% formamide and 50% 2XSSC at 65 °C for 1 hour and for Aβ antibody labeling with 50% formic acid in PBS for 30 minutes at room temperature. Sections were then treated with 1% H_2O_2 in PBS for 30 minutes, pre-incubated in 5% normal horse serum in PBS with 0.3% Triton X-100 for 1 hour, and then incubated with the primary antibodies at 4 °C overnight (see Table 1). Sections were further reacted with a biotinylated pan-specific secondary antibody (horse anti-mouse, rabbit and goat IgGs) at 1:400 for 2 hours, and subsequently with the ABC reagents (1:400) (Vector Laboratories, Burlingame, CA, USA) for another hour. Immunoreation product was visualized in 0.003% H_2O_2, 0.05% DAB, with (for BACE1) or without (for Aβ) enhancement in 0.025% NiCl and 0.025% CoCl. Three 10-minute washes were used between incubations. Sections were mounted on slides, allowed to air-dry and coverslipped.

Dual-chromogen double labeling was carried on selected sections (20 μm thick) from AD cases with mild to moderated plaque pathology to assess BACE1 and Aβ colocalization. BACE1 immunohistochemistry was processed first as described above, with the immunoreaction product visualized using DAB-nickel or DAB only. Following thorough PBS rinses and blocking excessive avidin/biotin binding sites using a commercial kit (Avidin/biotin blocking kit, SP-2001, Vector Laboratories), the sections were further immunostained for Aβ, which was visualized using DAB and the VIP substrate (SK-4600, Vector Laboratories), respectively. Dual (DAB/VIP) and single (DAB) chromogen labelings were also used to simultaneously detect BACE1 and collagen-IV immunoreactivities in the monkey and human cerebral cortex.

Double immunofluorescent labeling was carried out by incubating sections in PBS containing 5% donkey serum and a pair of the primary antibodies raised in different species (Table 1) overnight at 4 °C, followed by a 2 hour reaction at room temperature with Alexa Fluor® 488 and Alexa Fluor® 594 conjugated donkey anti-mouse, anti-rabbit or anti-goat IgGs (1:200, Invitrogen, Carlsbad, CA, USA). Sections were then counter-stained with Hoechst 33342 (1:50000), washed thoroughly, and mounted with anti-fading medium before microscopic examination.

CO and NADPH-diaphorase histochemistry

Cytochrome c oxidase (CO) histochemical stain was processed by incubating the sections (monkey occipital cortex) in 0.05% DAB, 0.02% cytochrome c oxidase, and 4% sucrose in 0.1 M phosphate buffer (pH 7.4) at 37°C in the dark for 4 hours. Subsequently, the sections were rinsed thoroughly with PBS at room temperature before mounting, dehydration and coverslippering.

Nicotinamide adenine dinucleotide phosphate diaphorase (NADPH-d) histochemistry was used to visualize nitrinergic neurons and processes. Based on its labeling of epithelial nitric oxide synthase (eNOS), NADPH-d histochemistry was also used in the present study to visualize vasculature (Yan et al., 1996). Sections were incubated in 0.05 M Tris-HCl buffered saline (pH 8.0, TBS) containing 0.3% Triton X-100, 1 mM β-NADPH-d, 0.8 mM nitroblue tetrazolium and 5% dimethyl sulfoxide for 2 hours at 37 °C. After thorough rinse in PBS, NADPH-d-stained sections were further immunohistochemically processed for other markers (BACE1, Aβ and neuronal phenotype or neurotransmitter markers) using the DAB/peroxidase method. All histochemical reagents were from Sigma-Aldrich (St. Louis, MO, USA).

NIH-PA Author Manuscript

NIH-PA Author Manuscript

NIH-PA Author Manuscript

Western blot

Frozen human cortical samples were homogenized by sonication in T-PER buffer (×10, w / v) (Pierce, Rockford, IL, USA) containing a cocktail of protease inhibitors (Roche, Indianapolis, IN, USA) at 4 °C for 10 minutes. Protein extraction in pre-fixed monkey temporal cortical samples was carried out in the same T-PER buffer but containing a high (4%) concentration of sodium dodecylsulfate polyacrylamide (SDS) and over a longer digesting time (30 minutes on ice) (Xiong et al., 2008), after removing sucrose from the tissue with several changes of PBS for a few days. Tissue extracts were centrifuged at 15,000 ***g***. Supernatants were collected and protein concentrations determined by DC protein assay (Bio-Rad Laboratories, Hercules, CA, USA). Twenty-five microgram of protein was run on each lane in 12% SDS-polyacrylamide gel electrophoresis (PAGE) gels. The polypeptides were electrotransferred to Trans-Blot pure nitrocellulose membranes (Bio-Rad Lab.). Nitrocellulose membranes were immunoblotted with antibodies to *p*-tau, BACE1, APP, APP β-CTF and β-tubulin-III at approximate concentrations (Table-1). Immunoblotting signal was visualized with horseradish peroxidase-conjugated goat anti-rabbit IgG (1:20000; Bio-Rad Laboratories) and the ECL Plus Western Blotting Detection Kit (GE Healthcare Life Sciences, Piscataway, NJ, USA). Immunoblot images were captured in a UVP Biodoc-it system (UVP, Inc., Upland, CA, USA).

Imaging, densitometry, data and statistical analysis

Sections were examined and imaged on an Olympus BX60 microscope equipped with a digital imaging system (MicroFire® CCD camera and software, Optronics, Goleta, CA). Digital images were captured using 4×, 10×, 20× and 40× objectives with numerical apertures of 0.1, 0.3, 0.7 and 0.85, respectively. Each original image contained 1200×1600 pixels. Images used for comparative densitometry were captured with an identical photographic setting. Optic densities (o.d.) of BACE1 and Aβ IR in the human cortex, expressed as digital light units (DLU)/mm^2, were measured in the same area of adjacent sections, defined by landmarks including blood vessels, using the rectangular interconnecting selection tool of the OptiQaunt 4.1 software (Parkard Instruments, Meriden, CT, USA). The sampled areas had a flat pial surface and composed of a ~2.5 mm-wide strip covering all cortical layers in depth (i.e., montages of 2-3 images). For each AD case, four cortical areas (2 gyral and 2 sulcal regions) around the inferior temporal gyrus were selected for densitometry. The average of optic densities from batch-processed control sections was used as the cut-off threshold to calculate specific densities in AD sections. BACE1 and CO reactivity in the monkey striate cortex were measured in the blob and inter-blob compartments in layer III/IVa as well as in the underlying white matter. Specific BACE1 and CO densities in the blobs and inter-blobs were calculated by using the white matter densities as cut-off levels. For western blot data, optic densities over the immunoblot bands were measured, and data were standardized according to β-tubulin levels in corresponding samples. A specific quantification method was designated to determine the degree of spatial proximity of BACE1-labeled neuritic profiles to blood vessels and relative to vascular distance or interval in general, which will be detailed in the Results section (with illustration). Means of measurements (including data normalized to appropriate references) were calculated and compared statistically using ANOVA, student's *t*-test or correlation analysis (Prism GraphPad, San Diego, CA). The minimal significant level of difference was set at $p < 0.05$. Figure panels were assembled with Photoshop 7.1, with brightness and contract adjusted as needed.

NIH-PA Author Manuscript

NIH-PA Author Manuscript

NIH-PA Author Manuscript

Results

Distribution of BACE1 IR in adult monkey cerebral cortex and hippocampal formation

Normal BACE1 expression pattern in representative primate forebrain structures was assessed in the plaque-free monkey (mid-age) brains by immunohistochemistry, using a rabbit antibody (anti-BACE1α) raised against the N-terminal 46-163 amino acids of human BACE1 (Zhang et al., 2009, 2010). Overall, BACE1 immunoreactivity (IR) appeared to occur in the neuropil and neuronal terminals, rather than somata or large neuronal processes, in the cerebral cortex (Fig. 1A), hippocampal formation (Fig. 1A-C), amygdala and striatum (not shown). In the neocortex, layers I and IV generally exhibited a noticeably lighter BACE1 IR relative to the remaining layers, with little IR occurred in the white matter (Fig. 1A). In the hippocampus, moderate neuropil reactivity was present over the stratum oriens to stratum radiatum in CA1 (Fig. 1A). In the dentate gyrus, strong and distinct BACE1 IR occurred in the hilus, which extended along the mossy fiber pathway ending sharply at the CA3 and CA2 border (Fig. 1A, C). By closer examination, a small amount of labeled plexuses in the hilus appeared to also extend across the granule cell layer (Fig. 1B). The neuropil reactivity in the molecular layer was noticeably denser in the inner (~1/3) than the outer (~2/3) sublamina (Fig. 1B).

In the rodent olfactory pathway BACE1 expression is inversely correlated with metabolic activity under normal conditions and following functional deprivation (Yan et al., 2007; Zhang et al., 2010). To explore whether such a relationship also exists in the primate cerebral cortex, we paid particular attention to BACE1 labeling relative CO reactivity in the striate cortex (area 17). BACE1 IR in area 17 was fairly intense in the supragranular layers, displaying a differential sublaminar distribution and a modular organization around layers III-IV (Fig. 1D, E). Thus, two moderately immunoreactive neuropil bands occurred over laminae III/IVa and IVcβ, respectively. In contrast, laminae IVb and IVcα expressed relatively weak BACE1 IR (Fig. 1D). This differential sublaminar pattern of BACE1 IR appeared to match with that of CO reactivity in an adjacent section (Fig. 1E, F). Of particular note, BACE1 IR in deep layer III and lamina IVa showed a periodic variation along the tangential direction, with regularly-spaced zones displaying high and low IR alternatively. By comparing labeling patterns between consecutive sections, the low and high BACE1 immunoreactive zones were found to overlap with the so-called CO blobs and inter-blobs, respectively (Fig. 1E-I). Densitometric analysis confirmed a negative correlation between BACE1 and CO reactivities among the blob and inter-blob zones ($r=0.713$, $p<0.001$) (Fig. 1J).

Elevation of BACE1 protein and product in AD human and aged monkey cerebral cortices

Western blot analyses were carried out using temporal cortical homogenates to confirm elevated levels of some AD-related protein products in pathologically verified AD (n=7) relative to control (n=7) human cortices, and in aged monkey cortices with (n=3), relative to those without (n=4), cerebral plaque pathology (no tauopathy was found in any of the examined monkey brains) (Fig. 2A, B). Levels of *p*-tau were dramatically increased in AD (896 ± 256%, mean ± S.D., same data presenting format below) relative to control (100 ± 29%) cases ($p=0.0047$, paired one-tail student's *t*-test, same data analysis method below). Blotted *p*-tau protein products largely migrated at 50-70 kd, but appeared to contain low molecular weight species or truncated forms that displayed a great individual variability (Santpere et al., 2006). Levels of APP holo-proteins and N-terminal fragments immunoblotted with the monoclonal antibody 22C11 were higher in AD (186 ± 31%) than control (100 ± 37%) human cortices ($p=0.0003$). Multiple variants of BACE1 protein, likely with varying degrees of glycosylation (Yan et al., 2007), were increased concurrently in AD relative to control. Thus, levels of the 70Kd, 54K and 46 Kd BACE1 proteins were 139 ±

NIH-PA Author Manuscript

NIH-PA Author Manuscript

NIH-PA Author Manuscript

16% vs 100 ± 34% (p=0.0101), 162 ± 35% vs 100 ± 8% (p=0.0003) and 163 ± 35% vs 100 ± 41% (p=0.003), respectively, in AD as compared to control cortical extracts. Likewise, levels of APP β-CTF were higher in AD (151 ± 50%) than control (100 ± 39%) extracts with statistically significant difference (p=0.026) (Fig. 2A, C). Consistent with BACE1 protein alteration in AD relative to control human cortex, levels of the fully glycosylated 70 kd and deglycosylated 46 kd BACE1 proteins were increased in aged monkey cortices with, relative to those without, microscopically detectable amyloid plaques, up to 283 ± 21 % (vs 100 ±23%, p=0.0012) and 303 ± 29% (vs 100 ± 20%, p=0.0012), respectively (Fig. 2B, C).

Anatomic and densitometric analyses of BACE1 and Aβ IR in AD cerebral cortex

Increased BACE1 IR (referred to as BACE1 “elevation” hereafter, relative to background staining and based on the above biochemical data) arranged as localized profiles were consistently detected in AD and aged monkey cortex that contained amyloid plaques immunolabeled by various antibodies targeting the N-terminal or C-terminal amino acids of the Aβ domain (Figs. 3A-H; 4). In contrast, BACE1 IR in control cortex appeared as diffuse neuropil reactivity (Fig. 1A-D) or faint background-like labeling (Fig. 3I). Several approaches were used to determine whether BACE1 elevation and Aβ deposition in AD and aged monkey cortex might be correlated, including by comparing labeled profiles between adjacent sections, by densitometric analysis and by double labelings.

In AD cortex with relatively mild plaque pathology (3 out of 7 cases), BACE1-labeled elements appeared to spatially match with amyloid plaques in adjacent sections (40 μm-thick) in most cases, particularly evident for the large-sized profiles (Fig. 3A-D). In AD cases with moderate to severe plaque pathology, the spatial correlation between individual BACE1 and Aβ labeled profiles were somewhat difficult to distinguish in adjacent sections at low magnification (Fig. 3E-H). However, in general BACE1-labeled profiles were more numerous in AD cortical sections with a greater load of Aβ IR. Quantitatively, the specific densities of BACE1 IR and Aβ IR matched narrowly in AD cases (case# 1, 2 and 6) with relatively mild plaque load. In AD cases with moderate and severe plaque pathology (case#3-5 and 7), specific densities of Aβ IR appeared to be higher as compared to that of BACE1 IR (Fig. 3J). Because the amount/density of amyloid plaques might vary from region to region in the same brain, we plotted BACE1 and Aβ densitometric data from all AD cases based on the measured cortical fields (4 fields per AD case). This analysis yielded an overall positive correlation (R^2=0.81, p<0.0001, two-tailed correlation analysis) between specific densities of BACE1 and Aβ across the quantified cortical regions regardless of individual AD cases (Fig. 3K).

In dual-chromogen double labeling preparations (20 μm-thick sections), BACE1 IR and Aβ IR often co-existed locally forming compact-like plaques in AD cortex with mild to moderate plaque lesions (Fig. 4A-C). BACE1-labeled profiles appeared to be swollen/sprouting processes that sometimes arranged in a rosette-like fashion and cycled around Aβ IR deposited as extracellular plaques. Between the large plaques, small spherical elements were labeled for BACE1, which were not clearly associated with extracellular Aβ IR (Fig. 4A-C, arrows). To understand the non-parallelism between BACE1 IR and Aβ IR in AD cases with relatively heavy plaque pathology, we compared their patterns in detail between adjacent sections using vasculature labeled with collagen-IV as landmarks (Fig. 4D, E). Although most Aβ-labeled amyloid plaques appeared to site-specifically colocalize with noticeably increased BACE1 IR (relative to plaque-free areas), BACE1-labeled elements was fewer, finer or more weakly stained around some Aβ plaques relative to others (circled areas in Fig. D, E). The Aβ plaques associated with sparse BACE1 IR was seemingly optimal for a morphological configuration of “burn-out” or aged compact plaques (Fiala et al., 2007; Zhao et al., 2007; Duyckaerts, 2009).

NIH-PA Author Manuscript

NIH-PA Author Manuscript

NIH-PA Author Manuscript

We attempted to profile BACE1 IR using double immunofluorescence in AD cortex, but encountered disturbing lipofuscin autofluorescence and could only obtained limited usable data (Fig. 4F-H). Based on pattern difference between lipofuscin and antibody fluorescent signals, it was possible to identify colocalization between BACE1 IR and the amyloid autofluorescence through the blue filter (Fig. 4F, H) or specific Aβ IR (Fig. 4I, J). BACE1 and *p*-tau immunoreactive neuritic profiles were sometimes present around the same compact-like plaques. However, there was no colocalization of BACE1 and *p*-tau in the same neurites (Fig. 4K-N).

Characterization of BACE1 relative to amyloid and neuritic changes in monkey cerebral cortex

Mirror sections (20 μm-thick) from the temporal lobe of aged monkey were stained for BACE1 and Aβ to confirm a localized occurrence of BACE1/Aβ expressing neuritic plaques. BACE1-labeled profiles appeared to colocalize in most cases with amyloid plaques presumably containing Aβ40 (Fig. 5A, B) and Aβ42 (Fig. 5C, D). The pattern of BACE1 IR in plaque-free areas, including the mossy fiber terminals, was otherwise comparable to that in normal monkey brain (Figs. 1A; 5A, C).

Double immunofluorescence was used to study the details of BACE1 IR relative to Aβ IR around plaques. BACE1 IR appeared to coexist locally with Aβ IR visualized by 3D6 (Fig. 5E-G), 12F4 (H, I) and 6E10 (not shown). Collectively, BACE1/Aβ double-labeled profiles resembled neuritic or compact plaques, with BACE1 IR occurred in dystrophic neurites whereas Aβ IR appeared most evidently as extracellular deposits (Fiala, 2007; Zhang et al., 2009). Thus, among the cored compact plaques, Aβ IR was very bright at the center but spread towards the periphery according to an overall high to low gradient in intensity. This pattern could be appreciated by simply using short and slightly longer exposure time for capturing the Aβ IR signal (Fig. 5H, I). Among the small or primitive (i.e., without a clear Aβ core) plaques, Aβ IR was relatively weak (therefore, better seen in images captured with a relatively longer exposure time) and appeared to intermingle with BACE1 IR (Fig. 5E-I, marked with cycles).

It should be emphasized that weak Aβ IR also existed inside the BACE1-labeled swollen neurites. In fact, this BACE1/Aβ coexistence could be easily assessed in isolated neuritic profiles that were not clearly associated with extracellular Aβ deposits (Fig. 5E-G, arrows). It should be also noted that isolated as well as clusterized BACE1-containing dystrophic neurites colocalized frequently with APP (22C11 labeling) (Fig. 4J-L) and presenilin-1 (PS1) as well (Fig. 4M, N).

We further confirmed that BACE1-labeled dystrophic neurites were axonal terminals from different types of neurons (Zhang et al., 2009). BACE1 IR did not colocalize with microtubule associated protein 2 (MAP2) (Fig. 6A-C), but they colocalized with synaptophysin (Fig. 6D-F). A subset of BACE1-labeled neurites were immunoreactive for vesicular glutamate transporter-1 (VGLUT1) (Fig. 6G-I), choline acetyltransferase (ChAT) (Fig. 6J-L2) and tyrosine hydrogenase (TH) (not shown). We also found partial colocalization of BACE1 IR with interneuronal markers in the dystrophic neurites, for examples, parvalbumin (Fig. 6M, M′) and NADPH-d (Fig. 7A-I). However, BACE1-labeled dystrophic neurites were rarely immunolabeled for γ-aminobutyric acid (GABA) transporter-1 (GAT1) (Fig. 5N, N′), which is enriched in GABAergic presynaptic terminals (Yan et al., 1997).

NIH-PA Author Manuscript

NIH-PA Author Manuscript

NIH-PA Author Manuscript

Paravascular distribution of BACE1-labeled dystrophic axons

The dual histochemical and immunohistochemical preparation yielded consistent and distinct BACE1 and NADPH-d reactivities in neuronal and vascular structures in the monkey cortex. Examining sections at various anterioposterior cerebral levels, we found that in all cortical regions a great majority of BACE1-labeled neurites, from small isolated swollen spherical elements or process-like structures to clusters of densely packed neurites, occurred in close proximity to blood vessels (Fig. 7A-J; Supporting Fig. 2A-F). In fact, many BACE1-labeled neurites and clusters were in direct contact with, extended across or coiled around blood vessels. NADPH-d reactive dystrophic processes coexisted with BACE1-labeled swollen/sprouting axons in many neuritic clusters, but in general constituted only a small part of the latter (Fig. 7B, C2, C7, C8, D-I). NADPH-d reactivity varied among the double-labeled dystrophic neurites, with labeling intensity ranging from dark to light blue. In the latter scenario, BACE1/NADPH-d colocalization was seen fairly clear in the double-labeled profiles (Fig. 7F, G). In the former scenario, the heavy nitroblue tetrazolium product masked BACE1 IR, however, this colocalization could be visualized by using shorter incubations for NADPH-d histochemistry prior to BACE1 immunolabeling (data not shown, but see Fig. 5J in Zhang et al., 2009). BACE1-labeled neurites, including those coexpressing NADPH-d, existed in neuron-sparse regions of the cortex, i.e., the white matter and layer I (Fig. 7H, I; Supporting Fig. 2A, C).

We cross-validated the paravascular distribution of BACE1-labeled dystrophic neurites to vasculature in the aged monkey (Fig. 8A-C) and AD human (Fig. 8D-G) cortical sections counterstained with collagen IV. In this preparation, the great majority of BACE1-labeled dystrophic axons or axonal clusters were also found to reside close to or in direct contact with blood vessels in sections at all fronto-occipital levels from all monkeys with cerebral plaques, and across the temporal lobe cortical areas in AD cases (with mild to moderate plaque pathology).

Quantitative analysis on spatial proximity of BACE1-labeled dystrophic axons to vasculature

A quantification method was designed to analyze the closeness of BACE1-labeled neurites and neuritic clusters to vasculature visualized by NADPH-d labeling of the vascular endothelium (Fig. 7J, K); Supporting Fig. 2G). Quantification was carried out in temporal cortical sections (Fig. 7K, L; Supporting Fig. 2G), with additional trials also performed in the frontal cortex of one monkey, which yielded similar results (Supporting Fig. 2E, F, H). For a given neuritic cluster, the longest and shortest vertical distances to the nearest blood vessel were measured using the Image-J software (NIH, Bethesda, MD, USA) in 10× images randomly taken from layers III to VI in the middle and inferior temporal gyri. For neuritic clusters either in contact with or extended across blood vessels, their shortest distance was defined by simply creating a short line around the vessel (Fig. 7K, insert), which would report as a small numeric figure. After converted the pixel unit lengths into actual lengths (in μm) and rounded the data by one point after zero, the shortest distances defined by the above manner all appeared as “0” in the Excel spreadsheet. To reflect the relative sizes of the neuritic clusters, the “diameter” of a given cluster was calculated by subtracting its shortest distance from longest distance. For measuring the distances between blood vessels, the equal dividing (diagonal, vertical and horizontal) lines were created in each image, and the intervals between adjacent vascular crossing-points along these lines were measured (Fig. 7J). This systematic vascular measurement was also carried out in comparable cortical regions of NADPH-d stained sections from three plaque-free aged monkeys. Details for the above measurements are summarized below (Table 2).

NIH-PA Author Manuscript

NIH-PA Author Manuscript

NIH-PA Author Manuscript

The longest and shortest vertical distances of the neuritic clusters to the nearest blood vessels ranged in average about 30-50 μm and 7-10 μm, respectively, in the analyzed monkey temporal cortex (Table 2). Over a third of the neuritic clusters had their shortest vertical distance equivalent to zero, implicating that they were in contact with or extended across blood vessels. Plotting the data as a function of the neuritic diameter, the shortest distance values distributed largely around the level of their mean, whereas the longest distance values shifted upwards, with the increase of neuritic diameter (Fig. 7K; Supporting Fig. 2G, H). The longest vertical distance of a neuritic cluster would reflect its greatest tendency away from the blood vessel. Therefore, we compared the longest distances of the neuritic clusters with vascular intervals. The mean longest distance was about one third of the mean vascular interval in the plaque-bearing monkey cortex, with statistically significant difference between two parameters (p=0.004, n=3; paired student's t-test). No difference in cortical vascular distances was found between aged monkeys with, as compared to whose without, cerebral plaque pathology (p=0.19, n=3; paired student's t-test) (Fig. 7L; Table 2).

Collagen-IV immunolabeling displays vasculature vividly (Kawai et al., 1990), although in dual BACE1/collagen-IV immunolabeling (Fig. 8A-G) the color-contrast (i.e., purple/brown immunoreaction products visualized with VIP/DAB substrates) between dystrophic neurites and vasculature was not as distinct as in BACE1/NADPH-d preparation (brown/blue) (Fig. 7A). Therefore, quantification was carried out in 15 microscopic fields at 20× magnification taken randomly across the temporal neocortex for each brain, by measuring the longest vertical distances of individual neuritic clusters to the nearby blood vessels and the vascular intervals intersecting the diagonal lines of the image, and by documenting whether a neuritic cluster was overtly in contact with vessels by visual judgment. This analysis included 3 aged monkeys and 3 AD cases (AD#1-3), because plaque-associated BACE1-labeled dystrophic neurites were often not distinct likely due to a “burn-out” effect in AD cases with more severer plaque pathology (AD#4, 5, 7) (Fig. 8G). Thus, in each analyzed brain, the average longest vertical distance was constantly shorter than the average vascular interval (p<0.001, one-way ANOVA for all cases). In addition, approximately 60% neuritic clusters appeared to be physically in contact with blood vessels (including crossing) based on visual scoring (Fig. 8H, I).

Discussion

A number of issues involving amyloid pathogenesis in the human brain are currently unclear. For examples, are plaque onset and development primarily driving by Aβ overproduction or impaired clearance? Where do the excessive Aβ products primarily derive from? And even more complicated, is Aβ accumulation a cause or a consequence of other AD-related neurological or pathological abnormalities? The presence of Aβ products predominantly in the extracellular space can cause puzzlement in the interpretation for their origin from and their effect to surrounding cellular components. Given the ultimate source of Aβ and derivatives being the APP β-cleavage pathway, correlative BACE1 and Aβ examination in primate material may allow a better assessment for AD-type cerebral amyloid pathogenesis.

Aβ overproduction might be the primary driving force for AD-type cerebral amyloidosis

Many biochemical studies have shown elevated BACE1 protein, enzymatic activity and immediate product in the brain and/or CSF in sporadic AD (Fukumoto et al., 2002; Holsinger et al., 2002; Li et al., 2004; Zhong et al., 2007; Ewers et al., 2008; Zetterberg et al., 2008; Hampel and Shen, 2009; Vassar et., 2009). In the present study we confirmed the increase of BACE1 proteins and β-CTF in aged monkey and AD human cortices relative to controls by western blot using anti-BACE1α and other antibodies (Yan et al., 2007). APP

NIH-PA Author Manuscript

NIH-PA Author Manuscript

NIH-PA Author Manuscript

levels are also higher in AD than control cortical homogenates. The concurrent BACE1 and APP elevations may facilitate Aβ overproduction.

Using mirror section preparation and double immunofluorescence, we evaluated the spatial relationship between BACE1 elevation and plaque distribution. Compared to control cortex that exhibits essentially diffuse neuropil reactivity, increased BACE1 IR occurs clearly and site-specifically in plaque-bearing primate cortex, and co-exists locally with Aβ IR in aged monkey cortex, and in AD cases with relatively mild plaque lesions. This increased BACE1 IR localizes to swollen and sprouting neuronal processes characteristic of dystrophic axons (Fiala, 2007), but also occurs in small and isolated swollen processes and spherical elements. Further, BACE1 IR in small and overt dystrophic neurites co-exists with increased APP and PS1 IR (relative to background) as well as weak Aβ IR. Comparing the patterns of BACE1 and Aβ IR among plaque profiles, Aβ IR appears to emerge and accumulate with the growth of the neuritic clusters. Therefore, localized extracellular (extra-axonal) Aβ accumulation might occur as a result of Aβ overproduction and release from the dystrophic axonal neurites co-expressing high levels of APP, BACE1 and possibly γ-secretase (Zhang et al., 2009).

Our densitometric analysis shows an overall correlation between specific densities of BACE1 IR and Aβ IR among the AD cases or across cortical areas irrespective of individual cases. However, BACE1 IR density may not match to the extent of Aβ density in presumed late- or end-stage AD samples. Also, by comparing labelings in adjacent sections, we noticed that the amount of BACE1 IR could be much less relative to Aβ IR among some plaque profiles. Thus, BACE1 IR associated with a fairly dense Aβ plaque may appear as a cluster of small dot-like or fibrous labelings. These findings imply that amyloid plaques may eventually evolve into a “burn-out” end stage (Fiala, 2007). In this case, the dystrophic neurites may have largely degenerated, causing a loss of BACE1 IR. In addition, Aβ deposition may occur as diffuse plaques that are thought not to be associated with overt dystrophic neurites (Duyckaerts et al., 2009). This may be another reason why BACE1 IR is less relative to Aβ IR in some AD samples. However, it would be of interest to explore if BACE1 elevation may occur in fine neuronal terminals around diffuse plaques, given its normal neuropil localization.

BACE1 elevation is associated with a progressive axonal pathology involving multi-type neurons

Double labelings for BACE1 with axonal and dendritic (SYN, GAP43, MAP2) markers show a clear localization of increased BACE1 IR to swollen/sprouting axon terminals, or axonal dystrophic neurites in transgenic mouse, aged monkey and AD human brains (Sheng et al., 2003; Zhao et al., 2007; Zhang et al., 2009, 2010). In aged monkey cortex, this aberrant BACE1 expression marks axonal pathology fairly robust. Thus, BACE1-labeled dystrophic axons exhibit a wide spectrum of morphology, from isolated spherical or process-like elements, to small rosette-like budding apparatus, and to large hollowed or multi-cavitied clusters. In BACE1/Aβ double immunofluorescence, Aβ IR is apparently greater around large relative to small neuritic clusters. However, Aβ IR around small neuritic clusters and isolated neurites is weak and may be not visible. This means that classifying plaques (satellite, diffuse and compact forms) based on Aβ staining alone may possibly underestimate the neuritic type (Duyckaerts et al., 2009). In other double labelings, a subset of BACE1-labeled neurites may colocalize with one or another neuronal phenotype/transmitter marker. It is worth noting that BACE-labeled dystrophic axons might not consistently express specific neuronal markers. For instance, while BACE1-labeled dystrophic neurites may co-express several interneuron markers (e.g., GAD67, PV, NADPH-d), they are rarely co-labeled for GAT-1, which is enriched in normal GABAergic terminals (Yan et al, 1997).

NIH-PA Author Manuscript

NIH-PA Author Manuscript

NIH-PA Author Manuscript

The finding that Aβ overproduction and potential accumulation occur early inside axon terminals might be of important pathophysiological relevance in light of the toxic effect of Aβ products on synapses (Li et al., 2009; Moreno et al., 2009; Nimmrich and Ebert, 2009). Indeed, genetic attenuation of BACE1 and PS1 expression appears to prevent formation of dystrophic neurites (and plague formation) and synapse dysfunction in transgenic models of AD (Vassar et al., 2009; Chow et al., 2010; De Strooper et al., 2010).

Whether amyloid and tau pathologies are parallel or interactive in AD pathogenesis remains unsettled (Schonheit et al., 2004; Price & Morris, 2004; Fiala, 2007; Duyckaerts et al., 2009). Because *p*-tau-containing neurites may occur around amyloid plaques (Duyckaerts et al., 2009), we wonder if they colocalize with BACE1. As with an earlier report using a different pair of antibodies (Zhao et al., 2007), we did not detect direct BACE1 coexistence with *p*-tau labeled with the PHF1 antibody in plaque-associated dystrophic neurites. Previous studies also show lack of colocalization between *p*-tau and APP (Wang and Munoz, 1995) or the synaptic vesicle-associated protein chromogranin (Thal et al., 1998) in dystrophic neurites. Taken together, it appears that *p*-tau-labeled dystrophic neurites are probably not axonal.

Neuritic plaques develop in close proximity to cerebral vasculature

It is well-established that senile plaques distribute preferentially around blood vessels (Miyakawa et al., 1982; Kawai et al., 1990), which has led to one hypothesis that cerebral Aβ deposits derive from vasculature or the periphery via blood (Fiala, 2007). We show here a clear association of paravascular amyloid plaques with BACE1-labeled dystrophic neurites and a lack of BACE1 IR in vascular components, implying a neuronal origin of these plaques. Most dystrophic neurites appear to be in direct contact with blood vessels, and quantitative data indicate that the longest distances of the neuritic clusters to the nearest vessels are significantly shorter than vascular intervals in aged monkey and AD human cortices. Obviously, the paravascular localization of dystrophic neurites is not a random phenomenon. Because small and isolated dystrophic neurites also occur in proximity to blood vessels, neuritic plaques appear to emerge and develop near vasculature (Zhang et al., 2009). In other words, our data imply that vascular/metabolic abnormalities might play an early role in AD-type cerebral amyloidosis (Kuhl et al., 1984; Hachinski and Munoz, 1997; Cohen et al., 2009; Rocchi et al., 2009). Future studies are needed to explore whether functional or structural vascular deficit, or both, may induce axonal pathology associated with BACE1 elevation and Aβ accumulation. Recent experimental data suggest that metabolic impairment may facilitate Aβ genesis via BACE1 (Cole and Vassar, 2009). For instance, energy inhibition or metabolic stress up-regulates BACE1 in vivo and promotes amyloid pathology in transgenic models of AD (Velliquette et al., 2005; Xiong et al., 2007). Of note, there exists a biological mechanism that might link neuronal hypoactivity to Aβ overproduction via BACE1. As shown here in the visual cortical columns of normal monkey and earlier in the olfactory pathway of rodents (Yan et al., 2007; Zhang et al., 2010), BACE1 expression in neuronal terminals is inversely correlated with metabolic activity under physiological conditions. Because cerebral metabolic rate is coupled with neuronal and synaptic activity (Sibson et al, 1998; Attwell and Laughlin, 2001; Jin and Kim, 2008), BACE1 elevation in paravascular axonal terminals might occur in partnership with neuronal hypoactivity because of functional impairment of the vascular system.

In summary, the present study shows that in aged monkey and AD human cerebral cortices BACE1 elevation occurs in the swollen and sprouting axonal terminals of the neuritic plaques. These dystrophic axonal neurites may originate from multiple types of neurons and they distribute selectively in close proximity to vasculature. These findings suggest a pathogenic link between vascular/metabolic deficits, multisystem axonal pathology and amyloid accumulation/deposition in sporadic AD.

NIH-PA Author Manuscript

NIH-PA Author Manuscript

NIH-PA Author Manuscript

Supplementary Material

Refer to Web version on PubMed Central for supplementary material.

Acknowledgments

This study was supported in part by Illinois Department of Public Health (X.X.Y.), National Institute of Health (1R21NS056371 to P.R.P., X.X.Y.), Southern Illinois University Center for Alzheimer's disease and related disorders (X.X.Y., P.R.P., R.G.S.) and intramural program of the National Institute on Aging (H.C.). We thank Elan Pharmaceuticals and Drs. Haruhiko Akiyama and Peter Davis for providing Aβ and *p*-Tau (PHF1) antibodies.

References

Attwell D, Laughlin SB. An energy budget for signaling in the grey matter of the brain. J Cereb Blood Flow Metab. 2001; 21:1133–1145. [PubMed: 11598490]

Boche D, Zotova E, Weller RO, Love S, Neal JW, Pickering RM, Wilkinson D, Holmes C, Nicoll JA. Consequence of Abeta immunization on the vasculature of human Alzheimer's disease brain. Brain. 2008; 131:3299–3310. [PubMed: 18953056]

Chow VW, Savonenko AV, Melnikova T, Kim H, Price DL, Li T, Wong PC. Modeling an anti-amyloid combination therapy for Alzheimer's disease. Sci Transl Med. 2010; 2:13ra1.

Chu Y, Kordower JH. Age-associated increases of alpha-synuclein in monkeys and humans are associated with nigrostriatal dopamine depletion: Is this the target for Parkinson's disease? Neurobiol Dis. 2007; 25:134–149. [PubMed: 17055279]

Cohen AD, Price JC, Weissfeld LA, James J, Rosario BL, Bi W, Nebes RD, Saxton JA, Snitz BE, Aizenstein HA, Wolk DA, Dekosky ST, Mathis CA, Klunk WE. Basal cerebral metabolism may modulate the cognitive effects of Abeta in mild cognitive impairment: an example of brain reserve. J Neurosci. 2009; 29:14770–14778. [PubMed: 19940172]

Cole SL, Vassar R. Linking vascular disorders and Alzheimer's disease: potential involvement of BACE1. Neurobiol Aging. 2009; 30:1535–1544. [PubMed: 18289733]

De Strooper B, Vassar R, Golde T. The secretases: enzymes with therapeutic potential in Alzheimer disease. Nat Rev Neurol. 2010; 6:99–107. [PubMed: 20139999]

Dickson TC, Vickers JC. The morphological phenotype of beta-amyloid plaques and associated neuritic changes in Alzheimer's disease. Neuroscience. 2001; 105:99–107. [PubMed: 11483304]

Duyckaerts C, Delatour B, Potier MC. Classification and basic pathology of Alzheimer disease. Acta Neuropathol. 2009; 118:5–36. [PubMed: 19381658]

Ewers M, Zhong Z, Bürger K, Wallin A, Blennow K, Teipel SJ, Shen Y, Hampel H. Increased CSF-BACE 1 activity is associated with ApoE-epsilon 4 genotype in subjects with mild cognitive impairment and Alzheimer's disease. Brain. 2008; 131:1252–1258. [PubMed: 18334538]

Fiala JC. Mechanisms of amyloid plaque pathogenesis. Acta Neuropathol. 2007; 114:551–571. [PubMed: 17805553]

Fukumoto H, Cheung BS, Hyman BT, Irizarry MC. Beta-secretase protein and activity are increased in the neocortex in Alzheimer disease. Arch Neurol. 2002; 59:1381–1389. [PubMed: 12223024]

Hachinski V, Munoz DG. Cerebrovascular pathology in Alzheimer's disease: cause, effect or epiphenomenon? Ann N Y Acad Sci. 1997; 826:1–6. [PubMed: 9329676]

Hampel H, Shen Y. Beta-site amyloid precursor protein cleaving enzyme 1 (BACE1) as a biological candidate marker of Alzheimer's disease. Scand J Clin Lab Invest. 2009; 69:8–12. [PubMed: 18609117]

Härtig W, Goldhammer S, Bauer U, Wegner F, Wirths O, Bayer TA, Grosche J. Concomitant detection of beta-amyloid peptides with N-terminal truncation and different C-terminal endings in cortical plaques from cases with Alzheimer's disease, senile monkeys and triple transgenic mice. J Chem Neuroanat. 2010 Mar 25. Epub ahead of print.

Holsinger RM, McLean CA, Beyreuther K, Masters CL, Evin G. Increased expression of the amyloid precursor beta-secretase in Alzheimer's disease. Ann Neurol. 2002; 51:783–786. [PubMed: 12112088]

NIH-PA Author Manuscript

NIH-PA Author Manuscript

NIH-PA Author Manuscript

Jin T, Kim SG. Cortical layer-dependent dynamic blood oxygenation, cerebral blood flow and cerebral blood volume responses during visual stimulation. Neuroimage. 2008; 43:1–9. [PubMed: 18655837]

Kawai M, Kalaria RN, Harik SI, Perry G. The relationship of amyloid plaques to cerebral capillaries in Alzheimer's disease. Am J Pathol. 1990; 137:1435–1446. [PubMed: 2260630]

Kawai M, Cras P, Perry G. Serial reconstruction of beta-protein amyloid plaques: relationship to microvessels and size distribution. Brain Res. 1992; 592:278–282. [PubMed: 1280517]

Kuhl DE, Metter EJ, Riege WH, Hawkins RA. The effect of normal aging on patterns of local cerebral glucose utilization. Ann Neurol. 1984; 15:S133–137. [PubMed: 6611114]

Li R, Lindholm K, Yang LB, Yue X, Citron M, Yan R, Beach T, Sue L, Sabbagh M, Cai H, Wong P, Price D, Shen Y. Amyloid beta peptide load is correlated with increased beta-secretase activity in sporadic Alzheimer's disease patients. Proc Natl Acad Sci U S A. 2004; 101:3632–3637. [PubMed: 14978286]

Li S, Hong S, Shepardson NE, Walsh DM, Shankar GM, Selkoe D. Soluble oligomers of amyloid Beta protein facilitate hippocampal long-term depression by disrupting neuronal glutamate uptake. Neuron. 2009; 62:788–801. [PubMed: 19555648]

Miners JS, van Helmond Z, Kehoe PG, Love S. Changes with age in the activities of beta-secretase and the Abeta-degrading enzymes neprilysin, insulin-degrading enzyme and angiotensin-converting enzyme. Brain Pathol. 201010.1111/j.1750-3639.2010.00375.x

Miyakawa T, Shimoji A, Kuramoto R, Higuchi Y. The relationship between senile plaques and cerebral blood vessels in Alzheimer's disease and senile dementia. Morphological mechanism of senile plaque production. Virchows Arch B Cell Pathol Incl Mol Pathol. 1982; 40:121–129. [PubMed: 6127830]

Moreno H, Yu E, Pigino G, Hernandez AI, Kim N, Moreira JE, Sugimori M, Llinás RR. Synaptic transmission block by presynaptic injection of oligomeric amyloid beta. Proc Natl Acad Sci U S A. 2009; 106:5901–5906. [PubMed: 19304802]

Mulder SD, van der Flier WM, Verheijen JH, Mulder C, Scheltens P, Blankenstein MA, Hack CE, Veerhuis R. BACE1 activity in cerebrospinal fluid and its relation to markers of AD pathology. J Alzheimers Dis. 2010; 20:253–260. [PubMed: 20164582]

Neugroschl J, Sano M. Current treatment and recent clinical research in Alzheimer's disease. Mt Sinai J Med. 2010; 77:3–16. [PubMed: 20101716]

Nimmrich V, Ebert U. Is Alzheimer's disease a result of presynaptic failure? Synaptic dysfunctions induced by oligomeric beta-amyloid. Rev Neurosci. 2009; 20:1–12. [PubMed: 19526730]

Portelius E, Bogdanovic N, Gustavsson MK, Volkmann I, Brinkmalm G, Zetterberg H, Winblad B, Blennow K. Mass spectrometric characterization of brain amyloid beta isoform signatures in familial and sporadic Alzheimer's disease. Acta Neuropathol. 201010.1007/s00401-010-0690-1

Price DL, Martin LJ, Sisodia SS, Wagster MV, Koo EH, Walker LC, Koliatsos VE, Cork LC. Aged non-human primates: an animal model of age-associated neurodegenerative disease. Brain Pathol. 1991; 1:287–296. [PubMed: 1688300]

Price JL, Morris JC. So what if tangles precede plaques? Neurobiol Aging. 2004; 25:721–723. [PubMed: 15165694]

Roth GS, Mattison JA, Ottinger MA, Chachich ME, Lane MA, Ingram DK. Aging in rhesus monkeys: relevance to human health interventions. Science. 2004; 305:1423–1426. [PubMed: 15353793]

Rocchi A, Orsucci D, Tognoni G, Ceravolo R, Siciliano G. The role of vascular factors in late-onset sporadic Alzheimer's disease. Genetic and molecular aspects. Curr Alzheimer Res. 2009; 6:224–237. [PubMed: 19519304]

Sani S, Traul D, Klink A, Niaraki N, Gonzalo-Ruiz A, Wu CK, Geula C. Distribution, progression and chemical composition of cortical amyloid-beta deposits in aged rhesus monkeys: similarities to the human. Acta Neuropathol. 2003; 105:145–156. [PubMed: 12536225]

Santpere G, Puig B, Ferrer I. Low molecular weight species of tau in Alzheimer's disease are dependent on tau phosphorylation sites but not on delayed post-mortem delay in tissue processing. Neurosci Lett. 2006; 399:106–110. [PubMed: 16488541]

Sarsoza F, Saing T, Kayed R, Dahlin R, Dick M, Broadwater-Hollifield C, Mobley S, Lott I, Doran E, Gillen D, Anderson-Bergman C, Cribbs DH, Glabe C, Head E. A fibril-specific, conformation-

NIH-PA Author Manuscript

NIH-PA Author Manuscript

NIH-PA Author Manuscript

dependent antibody recognizes a subset of Abeta plaques in Alzheimer disease, Down syndrome and Tg2576 transgenic mouse brain. Acta Neuropathol. 2009; 118:505–517. [PubMed: 19360426]

Schönheit B, Zarski R, Ohm TG. Spatial and temporal relationships between plaques and tangles in Alzheimer-pathology. Neurobiol Aging. 2004; 25:697–711. [PubMed: 15165691]

Sheng JG, Price DL, Koliatsos VE. The beta-amyloid-related proteins presenilin 1 and BACE1 are axonally transported to nerve terminals in the brain. Exp Neurol. 2003; 184:1053–1057. [PubMed: 14769400]

Sibson NR, Dhankhar A, Mason GF, Rothman DL, Behar KL, Shulman RG. Stoichiometric coupling of brain glucose metabolism and glutamatergic neuronal activity. Proc Natl Acad Sci U S A. 1998; 95:316–321. [PubMed: 9419373]

Thal DR, Hartig W, Schober R. Stage-correlated distribution of type 1 and 2 dystrophic neurites in cortical and hippocampal plaques in Alzheimer's disease. J Brain Res. 1998; 39:175–181.

Thal DR, Capetillo-Zarate E, Del Tredici K, Braak H. The development of amyloid beta protein deposits in the aged brain. Sci Aging Knowledge Environ. 2006; 6:re1. [PubMed: 16525193]

Thinakaran G, Koo EH. Amyloid precursor protein trafficking, processing, and function. J Biol Chem. 2008; 283:29615–29619. [PubMed: 18650430]

van Helmond Z, Miners JS, Kehoe PG, Love S. Oligomeric Abeta in Alzheimer's disease: relationship to plaque and tangle pathology, APOE genotype and cerebral amyloid angiopathy. Brain Pathol. 2010; 20:468–480. [PubMed: 19725829]

Vassar R, Kovacs DM, Yan R, Wong PC. The beta-secretase enzyme BACE in health and Alzheimer's disease: regulation, cell biology, function, and therapeutic potential. J Neurosci. 2009; 29:12787–12794. [PubMed: 19828790]

Velliquette RA, O'Connor T, Vassar R. Energy inhibition elevates β-secretase levels and activity and is potentially amyloidogenic in APP transgenic mice: possible early events in Alzheimer's disease pathogenesis. J Neurosci. 2005; 25:10874–10883. [PubMed: 16306400]

Welander H, Frånberg J, Graff C, Sundström E, Winblad B, Tjernberg LO. Abeta43 is more frequent than Abeta40 in amyloid plaque cores from Alzheimer disease brains. J Neurochem. 2009; 110:697–706. [PubMed: 19457079]

Weller RO, Preston SD, Subash M, Carare RO. Cerebral amyloid angiopathy in the aetiology and immunotherapy of Alzheimer disease. Alzheimers Res Ther. 2009; 1:6. [PubMed: 19822028]

Wang D, Munoz DG. Qualitative and quantitative differences in senile plaque dystrophic neurites of Alzheimer's disease and normal aged brain. J Neuropathol Exp Neurol. 1995; 54:548–556. [PubMed: 7602328]

Xiong K, Cai H, Luo XG, Struble RG, Clough RW, Yan XX. Mitochondrial respiratory inhibition and oxidative stress elevate beta-secretase (BACE1) proteins and activity in vivo in the rat retina. Exp Brain Res. 2007; 181:435–346. [PubMed: 17429617]

Xiong K, Huang H, Wang H, Cai Y, Yang J, Huang JF, Luo XG, Yan XX. β-Amyloid precursor protein cleavage enzyme-1 extracted from formalin-fixed, paraffin-embedded tissue following different sodium dodecylsulfate concentration treatment. Chinese J Anat. 2008; 31:761–763.

Yan XX, Jen LS, Garey LJ. NADPH-diaphorase-positive neurons in primate cerebral cortex colocalize with GABA and calcium-binding proteins. Cereb Cortex. 1996; 6:524–529. [PubMed: 8670678]

Yan XX, Cariaga WA, Ribak CE. Immunoreactivity for GABA plasma membrane transporter, GAT-1, in the developing rat cerebral cortex: transient presence in the somata of neocortical and hippocampal neurons. Dev Brain Res. 1997; 99:1–19. [PubMed: 9088561]

Yan XX, Xiong K, Luo XG, Struble RG, Clough RW. beta-Secretase expression in normal and functionally deprived rat olfactory bulbs: inverse correlation with oxidative metabolic activity. J Comp Neurol. 2007; 501:52–69. [PubMed: 17206602]

Zetterberg H, Andreasson U, Hansson O, Wu G, Sankaranarayanan S, Andersson ME, Buchhave P, Londos E, Umek RM, Minthon L, Simon AJ, Blennow K. Elevated cerebrospinal fluid BACE1 activity in incipient Alzheimer disease. Arch Neurol. 2008; 65:1102–7. [PubMed: 18695061]

Zhang XM, Cai Y, Cai H, Xiong K, Luo XG, Feng JC, Clough RW, Struble RG, Patrylo PR, Yan XX. BACE1 elevation in transgenic mouse models of Alzheimer's disease is associated with synaptic/axonal pathology and amyloidogenesis: implications for neuritic plaque development. Eur J Neurosci. 2009; 30:2271–2283. [PubMed: 20092570]

NIH-PA Author Manuscript

NIH-PA Author Manuscript

NIH-PA Author Manuscript

Zhang XM, Xiong K, Cai Y, Cai H, Luo XG, Feng JC, Clough RW, Patrylo PR, Struble RG, Yan XX. Functional deprivation promotes amyloid plaque pathogenesis in Tg2576 mouse olfactory bulb and piriform cortex. Eur J Neurosci. 2010; 31:710–721. [PubMed: 20384814]

Zhao J, Fu Y, Yasvoina M, Shao P, Hitt B, O'Connor T, Logan S, Maus E, Citron M, Berry R, Binder L, Vassar R. Beta-site amyloid precursor protein cleaving enzyme 1 levels become elevated in neurons around amyloid plaques: implications for Alzheimer's disease pathogenesis. J Neurosci. 2007; 27:3639–3649. [PubMed: 17409228]

Zhong Z, Ewers M, Teipel S, Bürger K, Wallin A, Blennow K, He P, McAllister C, Hampel H, Shen Y. Levels of beta-secretase (BACE1) in cerebrospinal fluid as a predictor of risk in mild cognitive impairment. Arch Gen Psychiatry. 2007; 64:718–26. [PubMed: 17548753]

NIH-PA Author Manuscript
NIH-PA Author Manuscript
NIH-PA Author Manuscript

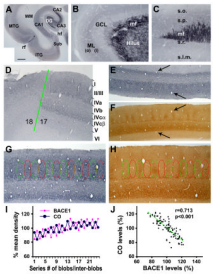

FIG. 1.

BACE1 immunoreactivity (IR) in normal monkey hippocampal formation (A-C) and visual cortex (images are from the 22 year-old animal). BACE1 IR occurs generally in the neuropil across the temporal lobe regions including the subiculum (Sub), inferior and medial temporal gyri (ITG, MTG) and hippocampus CA1 and CA2 sectors (A). BACE1 IR in the dentate gyrus (DG) distinctly delineates the mossy fiber (mf) pathway in the hilus extending along CA3 and ending at the CA3/CA2 border (B, C). The granule cell layer (GCL) shows faint labeling except for some mossy fibers from the hilus. The neuropil reactivity in the molecular layer (ML) is noticeable heavier in the inner (i) than the outer (o) portion of this layer (B). The laminar distribution pattern of BACE1 IR changes abruptly at the border between areas 17 and 18. In area 17 (striate cortex), BACE1 neuropil reactivity occurs as two bands over laminae II-IVa and IVcβ (D), a laminar pattern similar to that of cytochrome c oxidase (CO) reactivity (E, F). BACE1 IR in lamina III/IVa appears as regularly-spaced alternating zones/compartments with low and high intensities, which are complementary to CO reactivities in the blob and interblob zones (E-H). Optic densities (o.d.) in these lamina III/IVa compartments are measured first in CO sections, and the measuring templates are copied and then aligned over adjacent BACE1 sections coordinately (G, H). Specific BACE1/CO densities are calculated by using the BACE1/CO densities measured over the underlying white matter as cut-off thresholds. The resulting specific BACE1/CO densities in individual blob and interblob zones are normalized to the corresponding means of all zones, yielding the relative densities or levels (% of mean density) in individual zones. (I) Plots the relative densities of BACE1 and CO reactivities among 24 neighboring compartments from a representative section. (J) Shows a negative correlation ($r=0.713$, $p<0.001$) between BACE1 and CO levels among ~100 compartments measured in 2 sets of sections from each of the two youngest monkeys (22 and 23 year-old). Lamination of the striate cortex is marked on the right of (D). Arrows in (E, F) point to blood vessels. hf: hippocampal fissure; rf: rhinal fissure; s.o.: stratum oriens; s.p.: stratum pyramidale; s.r.: stratum radiatum; s.l.m.: stratum lacunosum-moleculare. Scale bar in (A) = 2 mm, equal to 100 μm for (B-D, G, H) and 200 μm for (E, F).

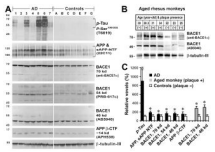

FIG. 2.

Immunoblotting of cortical samples from aged humans (n=14) (A) and monkeys (n=7) (B) confirming elevations of some Alzheimer's disease (AD) related proteins in diseased brains relative to controls (free of amyloid or tangle pathology). All data are normalized to the corresponding means (e.g., 100%) of the control groups. Levels of phosphorylated tau (*p*-Tau), full-length amyloid precursor protein (APP) and its N-terminal fragments (sAPP NTF), BACE1 proteins migrated at 70, 54 and 46 kd, and β-site cleavage APP C-terminal fragment migrated at ~14 kd are significantly higher in AD relative to control samples (C). Levels of the 70 and 46 kd BACE1 proteins are elevated in aged monkey cortices with cerebral plaques relative to plaque-free cases (C). *: $p<0.05$.

NIH-PA Author Manuscript NIH-PA Author Manuscript NIH-PA Author Manuscript

NIH-PA Author Manuscript

NIH-PA Author Manuscript

NIH-PA Author Manuscript

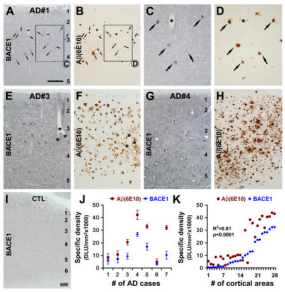

FIG. 3.

Comparative anatomical and densitometric analyses of BACE1 and Aβ (6E10) immunoreactivity (IR) in postmortem human cortex. (A-H) show representative images of BACE1 and Aβ IR in consecutive temporal cortical sections from AD cases with varying plaque pathology. BACE1-labeled profiles appear to match site-specifically with plaques in the cortex with relatively mild plaque load (A-D). In AD cortex with heavier amyloid loads, BACE labeled profiles appear to be less numerous relative to plaques (E-H). In control cortical sections, BACE1 (I) and Aβ (not shown) IR appears as weak and diffuse background staining. Therefore, the mean optic density of BACE1 or Aβ IR obtained from batch-processed control sections is used as the cut-off threshold to define the specific densities in the AD cortical sections (I, K). Panel (J) plots the specific densities (mean ± S.D., from 4 microscopic fields per brain) of BACE1/Aβ IR measured in the temporal cortex among the 7 AD cases. Panel (K) plots the same set of data by analyzed cortical fields, which yields an overall positive correlation (R^2=0.81, p<0.0001) between specific densities of BACE1 and Aβ IR in AD cortex regardless of individual cases. Asterisks in (A-F) indicate blood vessels used as landmarks to help identify profiles between consecutive sections. Scale bar=500 μm in (A) applying to (B, E-H, L), equal to 250 μm for (C, D), and 50 μm for (I).

NIH-PA Author Manuscript
NIH-PA Author Manuscript
NIH-PA Author Manuscript

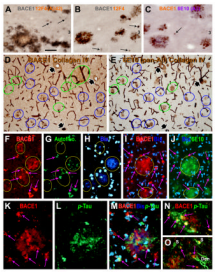

FIG. 4.

Double labeling for BACE1, Aβ and phospho-tau (*p*-Tau) in AD cortex. Panels (A-C) show examples of BACE1/Aβ colocalization in dual chromogen labeling. BACE1 IR may occur as small isolated spherical elements, which are not surrounded by extracellular Aβ deposits (pointed by arrows). In adjacent sections with the blood vessels (with 3 large ones indicated by fat arrows) co-stained by collagen-IV (D, E), BACE1 IR matches site-specifically with Aβ IR among most plaques profiles (green and blue cycles). However, some prominent Aβ plaques are associated less distinct BACE1 IR appearing as numerous dot-like or a few small process-like elements (compare profiles marked with green cycles between D and E, also see Fig. 8G). In double immunofluorescence, specific BACE1 labeling (yellow arrows) is seen through the red fluorescent filter only, whereas the lipofuscin autofluorescence (purple arrows) is strong but evident through both the red and green fluorescent filters (F, G). Of note, the amyloid core (yellow arrows) is visible through the blue fluorescent filter due to amyloid autofluorescence (H), especially by using a relatively long exposure time [(the bisbenzimide (Bis) nuclear stain is very bright in this case)]. Panels (I and J) show example of BACE1/Aβ colocalization in AD cortex that is distinguishable from non-specific autofluorescence (purple arrows). Panels (K-O) show a lack of colocalization between BACE1 and phosphorylated-tau (*p*-Tau) in plaque-associated dystrophic neurites. In contrast to BACE1-labeled counterparts, *p*-tau-labeled dystrophic neurites do not exhibit any consistency with regard to their amount, morphology and spatial relationship to/among the amyloid plaques (M-O). *p*-Tau-labeled somata and dystrophic-like dendrites also exist away from neuritic plaques (O). Scale bar=50 μm in (A) applying for (B, C, F-J), equal to 25 μm for (K-O), and 100 μm for (D, E).

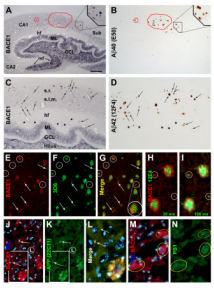

FIG. 5.

Representative images from a 34 year-old monkey showing colocalization of amyloidogenic proteins and β-amyloid peptides in dystrophic neurites and around neuritic plaques in the hippocampus (A-D) and neocortex (E-N). Panels (A-D) show colocalizations of BACE1 with Aβ40 (A, B) and Aβ42 (C, D) in consecutive hippocampal sections (20 μm thick). BACE1 ad Aβ labeled profiles are mostly present in the stratum radiatum (s.r.) and stratum lacunosum-moleculare (s.l.m.), and appear to match site-specifically in most cases between the two sections (examples are marked with frames and arrows). In double immunofluorescence, BACE1 labeling in dystrophic neurites coexists with local extracellular Aβ deposits visualized by 3D6 (E-G) and 12F4 (H, I). BACE1 and Aβ labelings interpose around virtually all primitive neuritic plaques (cycled profiles in E-I). A centroperipheral gradient of high to low Aβ IR around cored plaques is illustrated by using a short (30 miniseconds, H) and slightly longer (100 miniseconds, I) exposure for Aβ imaging. BACE1 and Aβ IR may colocalize inside small isolated swollen processes that are not surrounded by clear extracellular Aβ deposits (profiles pointed by arrows in E-G). BACE1 coexists commonly with amyloid precursor protein (APP) (J-L) and presenilin-1 (PS1) (M, N) in dystrophic neurites appearing as small “solid” as well as large “cavitied” clusters (J-N), or isolated swollen processes (arrows, in J). Bisbenzimide (Bis) nuclear counterstain is shown in blue in some images (J, L, M). Blood vessels (as labeled with asterisks in C, D) are used as landmarks to identify profiles between consecutive sections. Sub: subiculum; ML: molecular layer; mf: mossy fiber; GCL: granular cell layer; hf: hippocampal fissure. Scale bar=1.5 mm in (A) applying to (B), equal to 500 μm for (C, D), 250 μm for (E-G), 100 μm for (H-K, M, N) and 50 μm for (L).

NIH-PA Author Manuscript NIH-PA Author Manuscript NIH-PA Author Manuscript

NIH-PA Author Manuscript
NIH-PA Author Manuscript
NIH-PA Author Manuscript

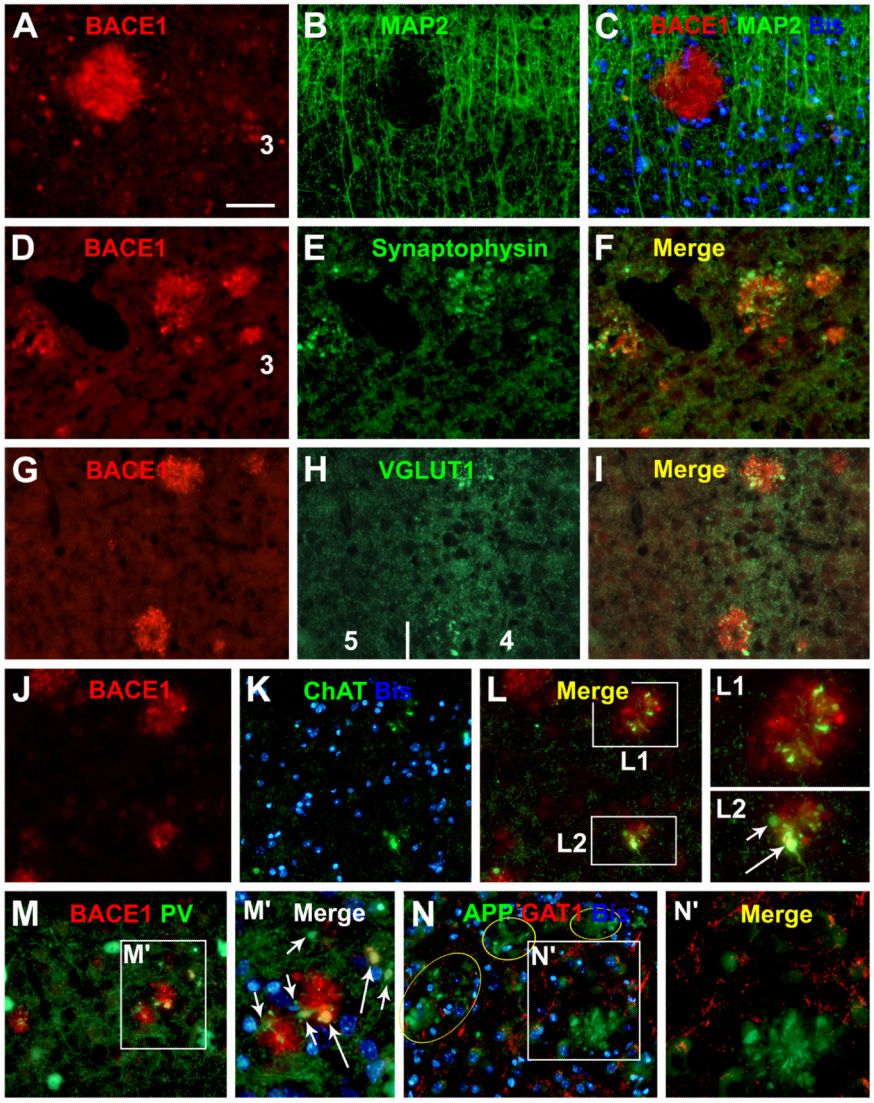

FIG. 6.

Localization of increased BACE1 IR to dystrophic axon terminals in aged monkey cortex. BACE1-labeled neurites do not colocalize with microtubule associated protein-2 (MAP2) (A-C), but colocalize with synaptophysin (D-F). A subset of BACE1-labeled dystrophic neurites coexpress vesicular glutamate transporter-1 (VGLUT1) (G-I), choline acetyltransferase (ChAT) (J-L2) and parvalbumin (M, M′). Note that the expression of the latter specific neuronal markers appears to be variable among the labeled neurites (examples are pointed by short and long arrows in I, L2, M′). γ-Aminobutyric acid (GABA) transporter-1 (GAT1) is barely detectable in BACE1-labeled dystrophic neurites (N, N′). Scale bar=100 μm in (A-L, M and N), and 50 μm for (L1, L2, M′ and N′).

NIH-PA Author Manuscript

NIH-PA Author Manuscript

NIH-PA Author Manuscript

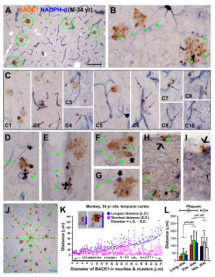

FIG. 7.

Paravascular distribution of BACE1-labeled dystrophic neurites in aged monkey cortex. Panels (A, B) show clusterized neurites apposing to and extending across blood vessels (marked with asterisks). Panels (C, C1-10) show examples of small neuritic clusters and isolated spherical or process-like elements (arrows) close to and coiling around blood vessels. Nicotinamide adenine dinucleotide phosphate diaphorase (NADPH-d) reactivity occurs in subset of BACE1-labeled neurites (B, C2, C7, C8, D-I), more clear in those with a lighter NADPH-d reaction (F, G). The dystrophic neurites are present in layer I (H, I). Panel (J) illustrates the method for quantifying blood vessel intervals by measuring the distances between neighboring vascular intersections along the equal-dividing (diagonal, horizontal and vertical) lines of the image. Image inserts in (K) show the method for measuring the longest and shortest vertical distances of individual neuritic clusters to the nearest blood vessel. The line graph (K) plots the longest and shortest distances of the measured clusters (n=237, with a diameter ≥ 5 μm) as a function of their diameters. Note the trend of upward shift of the longest distance with the increase of cluster size. The bar graph (L) summarizes the means of longest distances (long. dist.) and the vascular distances (vas. dist.) in the aged monkeys with (+, n=3) and without (-, n=3) cerebral plaques. Statistical analyses and results are indicated. Scale bar =100 μm in (A) applying to (H, I), equivalent to 50 μm for (B-G) and 250 μm for (J).

NIH-PA Author Manuscript

NIH-PA Author Manuscript

NIH-PA Author Manuscript

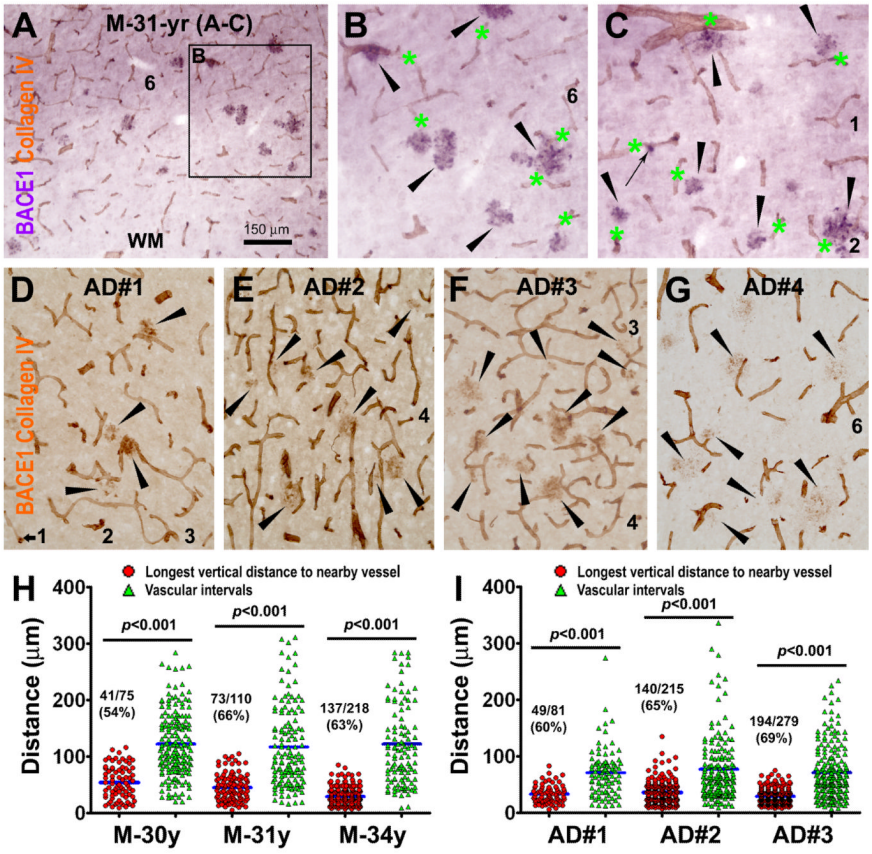

FIG. 8.

Analysis of the paravascular distribution of BACE1-labeled dystrophic neurites in aged monkey (A-C, H) and AD human (D-G, I) cortices in dual immunolabeling for BACE1 and collagen-IV. (A-C) show examples of VIP-visualized BACE1-expressing neuritic clusters (purple) tightly apposing collagen-labeled blood vessels (DAB reaction, brown) in a temporal cortical area of the 31-year old monkey (M-31-yr). Large and small neuritic clusters are pointed by arrowheads and a small arrow (B, C). In panels (D-G), BACE1 and collagen-IV immunoreactivities are concurrently visualized with the biotinylated horse IgG against mouse, rabbit and goat IgGs (Vector labs). BACE1-labeled neuritic clusters (arrowheads) occur around blood vessels (D-F). BACE1-labeled neurites appear as granule-like and short/small swollen elements around potential “burn-out” amyloid plaques especially in AD cases with heavier plaque pathology (G). Dot-graphs (H, I) show the numerical distribution of the longest vertical distances (red cycles) to the nearest blood vessels for individual neuritic clusters relative to vascular intervals (green triangles) intercrossing the diagonal lines measured in the same set of images. Mean comparisons (blue bars) yielded significant difference between the longest distances and vascular intervals in all analyzed monkey and AD cases. The ratio and percentage of neuritic clusters in contact with blood vessels (based on visual scoring) are given for each case. Scale bar=150 μm in (A) applying to (B, C) as 300 μm and (D-G) as 200 μm.

NIH-PA Author Manuscript

NIH-PA Author Manuscript

NIH-PA Author Manuscript

Table 1
Primary antibodies used in the present study

Antibody	Source	Product #	Dilution
mouse anti-Aβ1-5, 3D6	Elan	Lot#1132	(1:3000)
mouse anti-Aβ1-42, 12F4	Signet	39240	(1:2000)
rabbit anti-Aβ35-40	H. Akiyama	Ter-40	(1:3000)
mouse anti-Aβ1-16, 6E10	Signet	39320	(1:4000)
mouse anti-amyloid precursor protein, 22C11	Millipore	MAB348	(1:1000)
rabbit anti-amyloid precursor protein, C-terminal	Serotec	AHP538	(1:1000)
rabbit anti-BACE1α (a.a. residues 46-163)	H. Cai	anti-BACE1α	(1:2000)
rabbit anti-BACE1 (a.a. residues 485-501)	Convance	PRB-617c	(1:2000)
rabbit anti-BACE1 (a.a. residues 485-501)	Millipore	AB5940	(1:400)
mouse anti-calbindin	Sigma-Aldrich	C9848	(1:4000)
goat anti-choline acetyltransferase	Millipore	AB1447	(1:1000)
mouse anti-collagen, type IV	Sigma-Aldrich	C1926	(1:1000)
mouse anti-glutamic acid decarboxylase-67	Millipore	AB1511	(1:2000)
mouse anti-γ-aminobutyric acid transporter-1	Millipore	MAB5406	(1:4000)
mouse anti-growth- associated protein	Sigma-Aldrich	G9264	(1:4000)
mouse anti-microtubule associated protein-2	Sigma-Aldrich	M9942	(1:1000)
goat anti-presenilin-1	Sigma-Aldrich	P5235	(1:500)
rabbit anti-phospho-Tau (*p*-Ser199/Ser202)	Sigma-Aldrich	T6819	(1:3000)
mouse anti-phospho-Tau (*p*-Ser396/Ser404)	P. Davies	PHF1	(1:4000)
mouse anti-parvalbumin	Sigma-Aldrich	P3088	(1:4000)
mouse anti-synaptophysin	Millipore	MAB329	(1:4000)
rabbit anti-β-tubulin-III	Sigma-Aldrich	T2200	(1:10000)
mouse anti-tyrosine hydroxylase	Sigma-Aldrich	T2928	(1:4000)
mouse anti-vesicular glutamate transporter-1	Millipore	MAB5502	(1:2000)

NIH-PA Author Manuscript

NIH-PA Author Manuscript

NIH-PA Author Manuscript

Table 2
Summary of measurements for BACE1-labeled dystrophic neurites and blood vessels

Aged monkeys with cortical plaques	***M-30.3 yr-old***	***M-31 yr-old***	***M-34 yr-old***
Number of analyzed 10× temporal cortical images	12	12	12
Total number of measured neuritic clusters	205	245	237
Diameter of neuritic clusters (mean ± S.D., μm)	22.1 ± 14.8	42.4 ± 27.1	28.8 ± 19.2
Longest distance of neuritic clusters (mean ± S.D., μm)	28.8 ± 15.1	49.6 ± 29.1	38.6 ± 23.1
Shortest distance of neuritic clusters (mean ± S.D., μm)	6.8 ± 7.9	7.3 ± 9.3	9.9 ± 12.0
Neuritic clusters with shortest distance equal to zero (%)	45%	41%	34%
Vascular distance (mean ± S.D., μm)	106.6 ± 59.7	135.6 ± 65.4	121.8 ± 72.8
Total number of vascular intervals measured	356	375	289
Aged monkeys without cortical plaques	***M-25 yr-old***	***M-27 yr-old***	***M-30 yr-old***
Number of analyzed 10× temporal cortical images	12	12	12
Vascular distance (mean ± S.D., μm)	96.3 ± 59.2	125.3 ± 77.7	86.4 ± 66.9
Total number of vascular intervals measured	385	333	412